Compaction Wave Profiles: Simulations of Gas Gun Experiments

Ralph Menikoff
Theoretical Division, Los Alamos National Laboratory

Meso-scale simulations of a compaction wave in a granular bed of HMX have been performed. The grains are fully resolved in order that the compaction — porosity behind the wave front — is determined by the elastic-plastic response of the grains rather than an empirical law for the porosity as a function of pressure. Numerical wave profiles of the pressure and velocity are compared with data from a gas gun experiment. The experiment used an initial porosity of 36%, and the wave had a pressure comparable to the yield strength of the grains. The profiles are measured at the front and back of the granular bed. The transit time for the compaction wave to propagate between the gauges determines the wave speed. The wave speed depends on the porosity behind the wave and is affected by the strength model. The yield strength needed to match the experimental wave speed is discussed. Analysis of the lead wave through the granular bed, based on impedance matches using the Hugoniot loci, indicates that the compaction wave triggers a small amount of burn, less than 1% mass fraction, on the micro-second time scale of the experiment.

I. INTRODUCTION

Granular explosives are used as a model for damaged explosives. Damage gives rise to porosity and greatly increases the ignition sensitivity. Sensitivity is determined by the formation of hot spots when a compressive wave propagates in a heterogeneous medium. Hot spots are subgrain in extent and evolve on a fast time scale. Typically, the spatial scale is on the order of microns and the temporal scale is on the order of micro-seconds. Meso-scale simulations — continuum mechanics calculation which resolve individual grains — are currently the only means of obtaining detailed information on the small spatial and temporal scales which control the buildup and transition to a detonation wave.

As a test that the simulations capture the mechanical response of a heterogeneous material, we compute a propagating compaction wave in a granular bed of the explosive HMX (cyclo-tetramethylene-tetranitramine) and compare with experimental data of the wave profile. The wave strength in the experiments have a pressure comparable to the yield strength. In this regime most of the porosity is squeezed out but the temperature of the hot spots is low enough to treat the HMX as inert.

The compaction wave experiment are described in [1]. The experimental setup is shown in figure 1. A Kel-F projectile is accelerated by a gas gun and impacts a target assembly consisting of a front disk of Kel-F, a granular bed of HMX and a back disk of TPX. For the case considered here, the projectile velocity is 288 m/s and the bed is composed of crystals with a mean particle size of 120 μm and a porosity of 36%.

The experiment is designed to be one-dimensional. A wave diagram is shown in figure 2. Gauges at the front and back interface of the granular bed measure the time histories of either the pressure or the velocity. A pair of experiments is used to obtain both quantities. The front gauge captures the profile as the incident shock in the front disk matches into the granular bed and the profile of the return wave reflected from the back interface of the granular sample. The back gauge captures the profile when the compaction wave reflects off the interface between the granular bed and the back disk. The transit times between the signals at the front and back gauges determine the speeds of the incident and reflected waves in the granular bed. The wave speeds and wave profiles will be compared with the results of simulations.

Meso-scale simulations of the experiments are performed with an Eulerian continuum mechanics code developed by David Benson at the University of California, San Diego. A similar code has been used previously to study sintering or dynamic compaction of powdered metals [2,3]. Here we are considering weaker waves with a stress comparable to the yield strength, and aim to compare quantitatively with experimental data.

The grains are modeled as an isotropic elastic-plastic material. Compression of the granular bed leads to stress concentrations at the contact between grains. When the stress concentrations exceed the yield strength, the grains deform plastically. The change in the shape of the grains allow them to pack more tightly together and decreases the porosity of the bed. For a compaction wave, the value of the yield strength affects the change in porosity across the wave front, and the porosity behind the wave affects the wave speed. The first

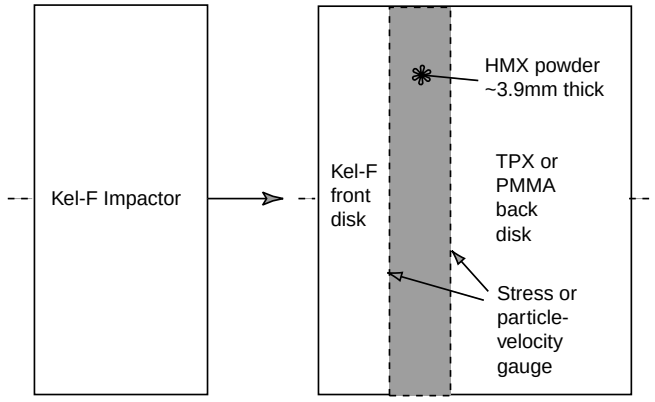

FIG. 1. Schematic of compaction wave experiment from [1]. The impactor is projectile from gas gun. Target assembly consists of granular sample of HMX between a front disk of Kel-F and a back disk of TPX.

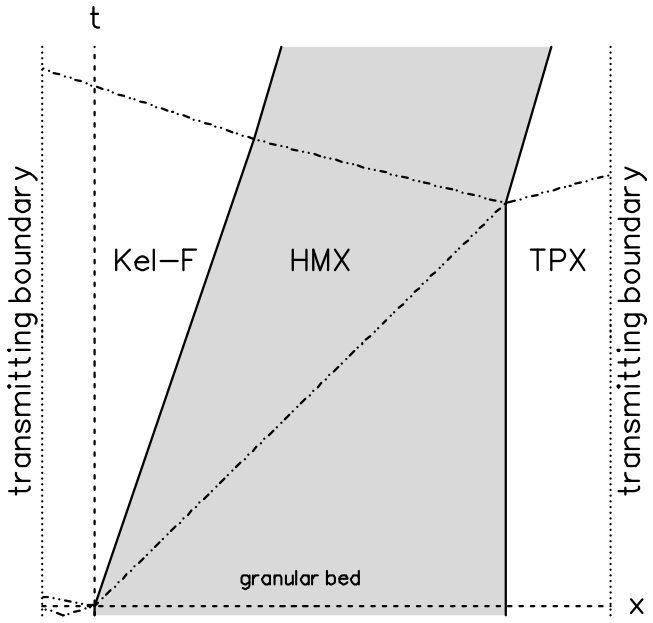

FIG. 2. Wave diagram of flow generated by gas gun experiment. Granular sample shown in gray and wave fronts as dot-dot-dashed lines.

finding of the simulations is that matching the compaction wave speed requires a low value of the yield strength compared to the value inferred from single crystal experiments. The discrepancy is related to the size distribution of the grains and the dimensionality (two-dimensional simulations for three-dimensional grains), both of which affect the structure of the granular bed.

A second finding is that the strength of the reflected wave from the back of the sample is lower in the simulation than the back gauge data of the experiment. Moreover, the gauge data is not compatible with impedance matches based on the shock Hugoniots of shock compressed HMX and the TPX backing. The discrepancy can be explained by assuming a small amount of burn, less than 1% mass fraction, which would increase the strength of the compaction wave as it propagates between the front and the back gauges. The small amount of burn is compatible with deflagration-to-detonation experiments on granular HMX [4] which show on a longer time scale than the gas gun experiment ($100\,\mu$s compared to $8\,\mu$s) that a compaction wave of the same strength (generated by a 200 m/s piston) transits to a detonation wave. Thus, there is experimental evidence that hot spots generated by even weak compaction wave are strong enough for some decomposition to occur on a micro-second time scale. However, due to the limited numerical resolution — 1% burn fraction corresponds to roughly 1 cell per grain — it is not possible to calculate accurately small amounts of burn, and the simulations discussed here treat the grains as inert.

The setup for the simulation is described briefly in section II. Results of the simulations and a comparison with the experimental data are presented in section III. The impedance match is analyzed in section IV. The analysis demonstrates that a small amount of burn is needed for consistency of the

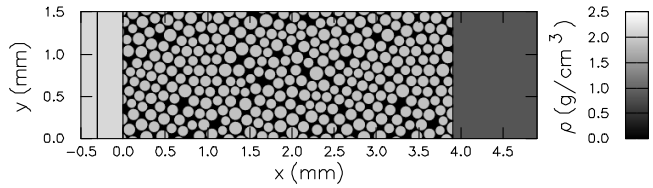

FIG. 3. Initial configuration for simulation. Granular bed has 36% porosity. Black regions are voids and represent pores between grains. Leftmost region is given an initial velocity corresponding to the projectile from the gas gun.

experimental data. We conclude in section V with remarks on the yield strength and issues with including reaction in simulations. Just as simulations of waves in a heterogeneous material are sensitive to modelling details, such as yield strength and granular structure, simulations of reactive materials will be sensitive to additional aspects of the model, such as dissipative mechanisms. Nevertheless, reactive simulations are needed to understand initiation mechanisms, and additional work is warranted.

II. NUMERICAL MODEL

The initial configuration for the two-dimensional simulations are shown in figure 3. The computational domain is $5.4\,\text{mm}\times1.5\,\text{mm}$. It consists of three region: the Kel-F front disk, $-0.5 < x < 0\,\text{mm}$; the porous sample, $0 < x < 3.9\,\text{mm}$; and the TPX back disk, $3.9 < x < 4.9\,\text{mm}$. The front disk is split into two regions. The flow is started by giving the leftmost region an initial velocity corresponding to the velocity of the projectile from the gas gun, 288 m/s. This allows the incident shock in the front disk to form before interacting with the sample. A transmitting left boundary allows reflected waves to escape, and mimics the effect of a larger front disk. The top and bottom edges have reflecting boundary conditions.

The grains of the sample are randomly distributed and correspond to a loosely packed bed. Circular grains are used with a diameter of $0.12\,\text{mm}\pm10\%$. The cell size used for the simulations is 10 microns, which corresponds on average to 12 cells in a grain diameter.

A hydrostatic equation of state (EOS) plus an elastic-plastic strength model are used for the constitutive relation of the HMX grains. The EOS is of the Mie-Grüneisen form with a reference curve based on a linear u_s–u_p fit to the principal shock Hugoniot. The strength model is isentropic with a constant shear modulus and von Mises yield strength for rate independent plasticity. A Mie-Grüneisen EOS is also used for the Kel-F and TPX. The parameters are listed in table I. The packing algorithm, constitutive relations and previous compaction wave simulations are described in [5,6].

Two columns of Lagrangian tracer particles (one particle per cell in the y-direction) are included in the simulations. The columns are located one cell from the interfaces with the granular bed; the front column in the Kel-F and the back column

TABLE I. Constitutive parameters for materials.

	HMX	Kel-F	TPX		
c_0	2.65	2.03	2.17	km/s	Bulk sound speed
s	2.38	1.64	1.52	—	Slope of u_s–u_p relation
Γ/V	2.09	2.33	0.91	g/cm^3	Grüneisen coefficient
ρ_0	1.9	2.12	0.83	g/cm^3	Initial density
G	12.	—	—	GPa	Shear modulus
Y	0.26	—	—	GPa	Yield strength

in the TPX. The values of the velocity and stress at each tracer particle in a column are averaged in order to compare with the gauge data.

III. COMPARISON WITH EXPERIMENTS

The first simulation used a value of the yield strength (2.6 kb) inferred from wave profile experiments in a single crystal of HMX [7,8]. The stress field and porosity profile of the compaction wave are shown in figure 4. Due to the material heterogeneities, the stress field is not uniform. Stress concentrations arise at the contacts between grains. When the stress concentrations exceed the yield strength, the grains deform plastically and squeezes out some of the pore space. In this case the porosity behind the wave is between 2 and 4%. Despite the fluctuations, the average stress profile is quite similar to a wave in a homogeneous material. However, the rise time depends on the grain structure and is not as narrow as would be the case for a shock wave in a homogeneous material.

A comparison with the gauge data [1, fig. 2.7] is shown in figure 5. The compaction wave speed in the simulation is too fast, and leads to a 0.2 μs timing error at the back gauge. This can be understood by examining the Hugoniot jump conditions for a porous medium.

The conservation of mass, momentum and energy can be expressed as

$$J\left[\phi\rho(u_p-u_s)\right]=0 \qquad (1)$$

$$J\left[\phi\rho(u_p-u_s)^2+\phi P\right]=0 \qquad (2)$$

$$J\left[\phi\rho(u_p-u_s)\left(e+0.5\,(u_p-u_s)^2+P/\rho\right)\right]=0 \qquad (3)$$

where ρ is the density of the grains, ϕ is the volume fraction of the grains, u_p is the particle velocity, u_s is the wave speed, e is the specific internal energy and $P=P(\rho,e)$ is the pressure within a grain and $J[Q]$ is the jump in Q across the wave front. Because of the additional degree of freedom associated with the porosity, to obtain the Hugoniot locus, the jump conditions must be supplemented with a compaction law of the form

$$P=\beta(\phi)\ . \qquad (4)$$

Without knowing the compaction law, one can still relate the wave speed to the porosity behind the wave.

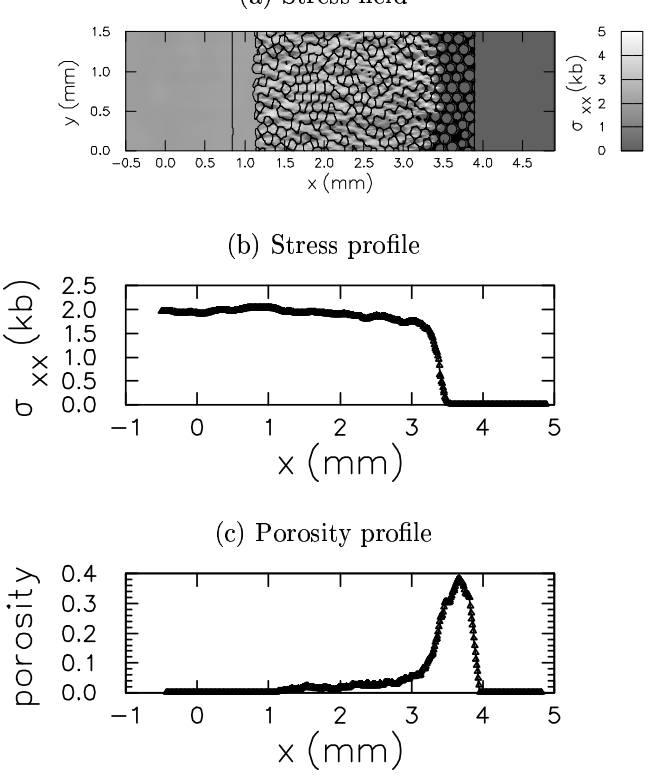

FIG. 4. Compaction wave before front ($x\approx 3.4$ mm) reaches the back of the sample ($x=3.9$ mm); time of 5 μs. Black regions in stress field are voids and represent pores between grains. Profiles are averages in the y-direction, *i.e.*, transverse to the wave propagation. In addition, the porosity profile is smoothed by taking a running average in the x-direction over a distance of 1 grain.

A material can support a non-zero porosity ($\phi<1$) only for $P\lesssim Y$. Typically, the yield strength Y is much less than the bulk modulus. Thus, when the porosity is non-zero, it is a good assumption that ρ is constant and the compression in a compaction wave is due to the change in ϕ. In this case, the jump condition for mass conservation reduces to

$$u_s=\frac{u_p}{1-\phi_0/\phi}\ . \qquad (5)$$

Hence, for a given piston velocity u, the wave speed decreases as the porosity $(1-\phi)$ behind the wave decreases.

To be quantitative, one can solve for the Hugoniot locus using the HMX equation of state and the compaction law based on the quasi-static compression data of Elban & Chiarito [9], shown in figure 6. From the front gauge, the velocity behind the compaction wave is 0.22 mm/μs. With this particle velocity, the wave speed as a function of porosity is shown in figure 7.

Based on the transit time from the gauge data (5.9 μs) and the length of the sample 3.9 mm, the compaction wave speed is 0.66 mm/μs. We then infer from figure 7 that the porosity behind the wave is nearly zero. This is smaller than the computed porosity in the simulation.

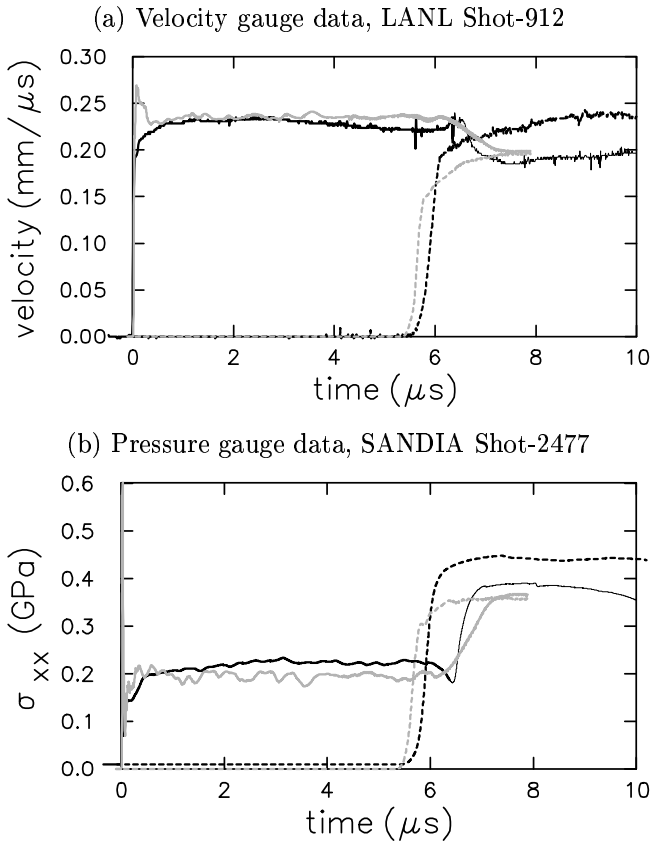

FIG. 5. Comparison between experiment [1, Fig. 2.7] and simulation using a yield strength of 2.6 kb. Black lines are gauge data. Thin line indicates possible contaminated with side rarefactions. Grey lines are from tracer particles in simulation with yield strength of 2.6 kb.

The porosity behind the wave depends on the yield strength and also the shear modulus. A lower yield strength decreases the porosity and hence lowers the wave speed. In the next simulation, the yield strength is lowered to 1 kb. This is sufficiently low to obtain a small porosity behind the compaction wave. The comparison with the gauge data for this case is shown in figure 8. It can be seen that the transit time of the compaction wave is now in good agreement with the experiment. Moreover, the transit time of the reflected wave is also fairly close.

Conversely a higher yield strength increases the porosity and increases the wave speed. A simulation using a yield strength of 3.7 kb resulted in 10% porosity and timing error of 1 μs for the signal at the back gauge. The important point is that the porosity behind a compaction wave can be determined by measuring the wave speed. The question of why a low yield stress is needed to obtain the measured porosity will be discussed later.

Though the wave speeds are in good agreement, there are three significant discrepancies in the comparison between the simulations and the gauge data. The first is the overshoot in the profile at the front gauge of the simulation compared to the data. The second is the low velocity and low stress at the back gauge in the simulation compared to the data. The third

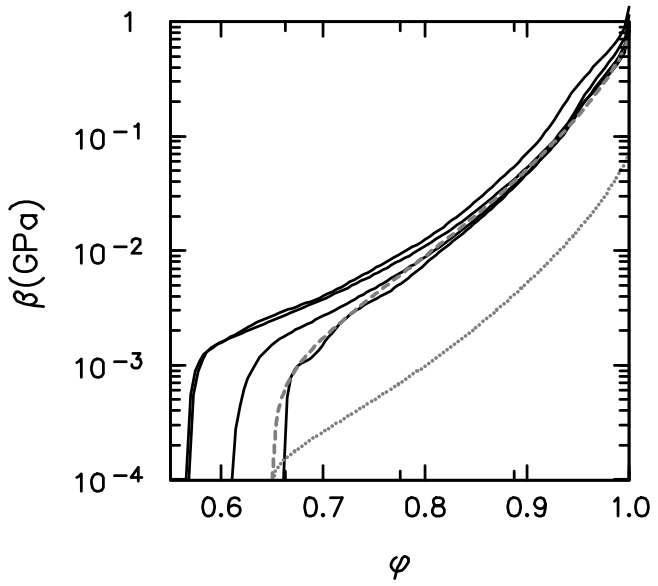

FIG. 6. Quasi-static compression data. Solid lines are data from Elban & Chiarito [9]. Dashed grey line is fit used for calculating porous Hugoniot. Dotted grey line is artificially lowered configuration pressure in order to obtain full compaction behind wave front.

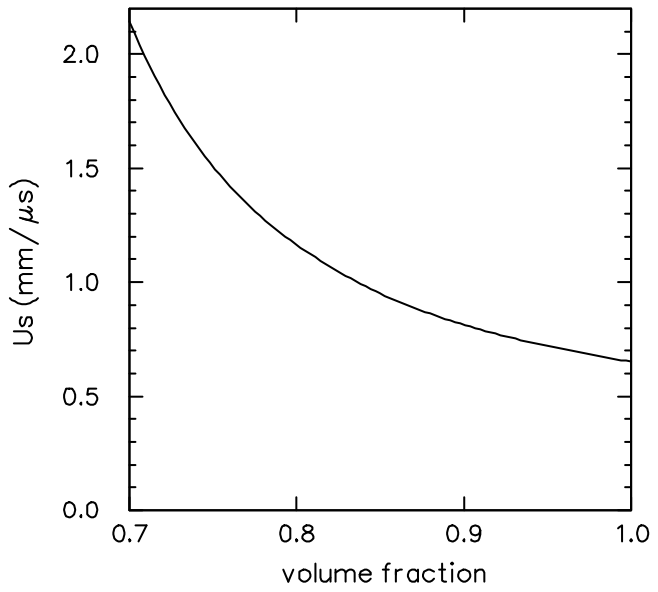

FIG. 7. Variation of wave speed with volume fraction behind compaction wave with a particle velocity of 230 m/s.

is the slow variation in the experimental record at the front gauge compared to the nearly constant time histories in the simulation. We next discuss these issues.

From the initial configuration shown in figure 3, we see that the grain packing results in some pores adjacent to the interface with Kel-F. As a consequence, when the incident shock wave matches into the granular bed, some Kel-F is blown off

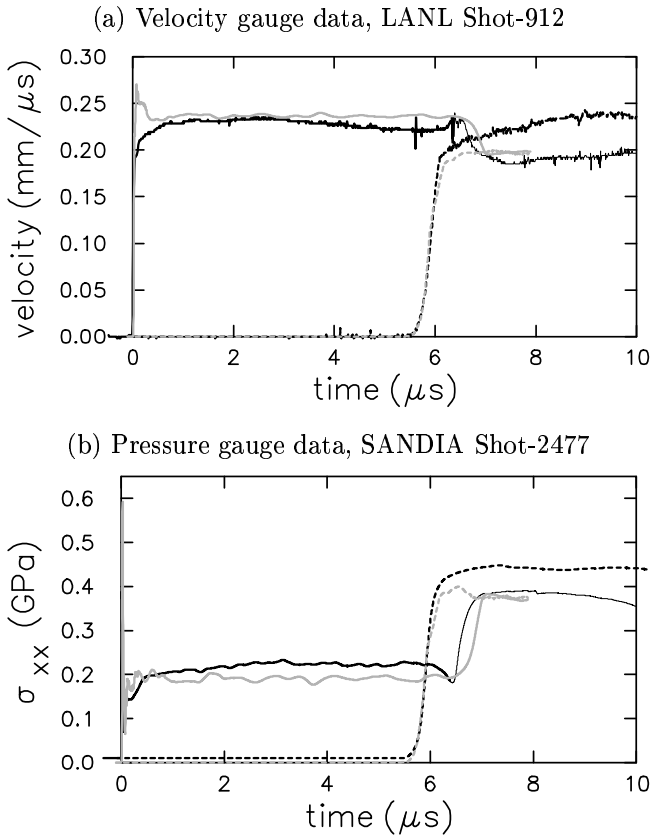

FIG. 8. Comparison between experiment and simulation that uses reduced yield strength. Black lines are gauge data. Thin line indicates possible contaminated with side rarefactions. Grey lines are from tracer particles in simulation with low yield strength of 1 kb.

the surface into the pores. This is seen in an expanded view of the interface shown in figure 9. Thus, a transient occurs while the compaction wave profile is forming in which the particle velocity of the material opposite the pores increases rather than matching down as is the case for the material adjacent to the grains. After the wave profile is formed, the interface settles down to a uniform velocity. Averaging the tracer particles results in a overshoot which then decays to the particle velocity behind the compaction wave.

The granular bed in the experiment has a distribution of grain sizes. Very likely small grains fill in the pores at the interface. In addition, the Kel-F is visco-elastic and a shock has a profile with a non-zero width. The combined effects very likely are sufficient to explain the difference in the velocity profile at the front gauge during the rise time of the compaction wave.

The transient peak in the simulated pressure profile at the front gauge corresponds to the pressure of the incident shock in the Kel-F. The experimental profile has a lower peak due in part to the response time of the pressure gauge, the match into the gauge materials and also the width of the incident shock. The simulation does not have the resolution to model accurately the gauges or the small grains in the size distribution.

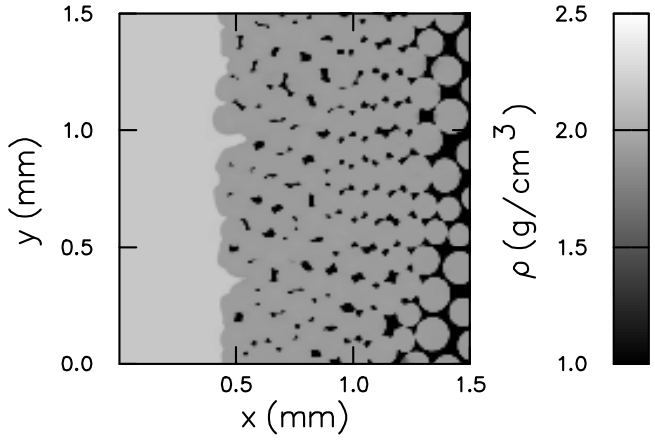

FIG. 9. Expanded view of interface adjacent to front gauge at early time ($2\,\mu$s). Light grey corresponds to Kel-F front disk, dark grey to HMX, and black regions to voids or pores between grains. Compaction front is at about $x = 1$ mm.

Thus, the simulation can not be expected to capture the transient behavior of the shock match into the granular bed. After the compaction wave is formed, the simulation does agree with the values behind the front reasonably well.

IV. IMPEDANCE MATCH

To understand the low values of the pressure and velocity in the simulation compared to the back gauges in the experiment, we study the impedance match of the compaction wave in the granular HMX with the back disk of TPX. The wave curves, in the (velocity, stress)–plane for the graphical solution to the impedance match problem, are shown in figure 10. Two cases are displayed. The black lines represent the porous Hugoniot with the compaction law based on the quasi-static experiments while the grey lines represent an artificially softened compaction law in order to achieve full compaction (zero porosity) for the compaction waves of interest. These two cases correspond to the configuration pressure given by the dashed and dotted grey curves in figure 6. The main difference is that the slope of the reflected wave curve (solid lines in figure 10) is larger when the granular bed is fully compacted. The fully compacted case is consistent with the simulation using the lower yield strength (corresponding to the softened compaction law) but not with the experiment. The slight difference with the simulation is due to neglecting the contribution from the stress deviator in computing the porous Hugoniot locus.

In general it follows from the slope of the wave curves that for an impedance match the velocity decreases when the stress increases. Yet the experimental velocity for the reflected wave is slightly higher than the velocity of the incident compaction wave. The impedance match is based on the assumption that the compaction wave does not change strength as it propagates across the sample. The

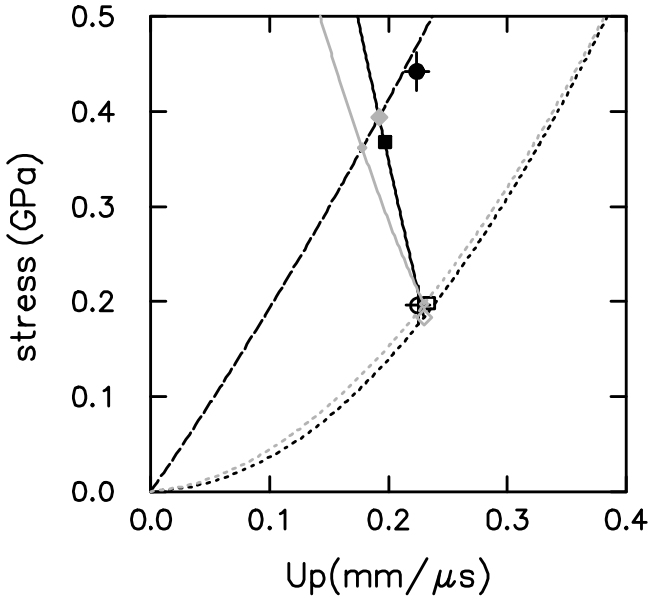

FIG. 10. Wave curves for impedance match at back interface of sample. Short dashed lines are Hugoniot loci in porous HMX. Long dashed line is shock locus for TPX. Solid lines are reflected Hugoniot loci in shock compressed sample. Black lines computed with experimental compaction law and grey lines with low configuration pressure in order that waves of interest are fully compacted. Solid and open symbols correspond to incident and reflected states. Black circles and squares represent experimental data and values from simulation, respectively. Grey diamonds represent impedance match, with large and small symbols corresponding to high and low configuration pressure, respectively.

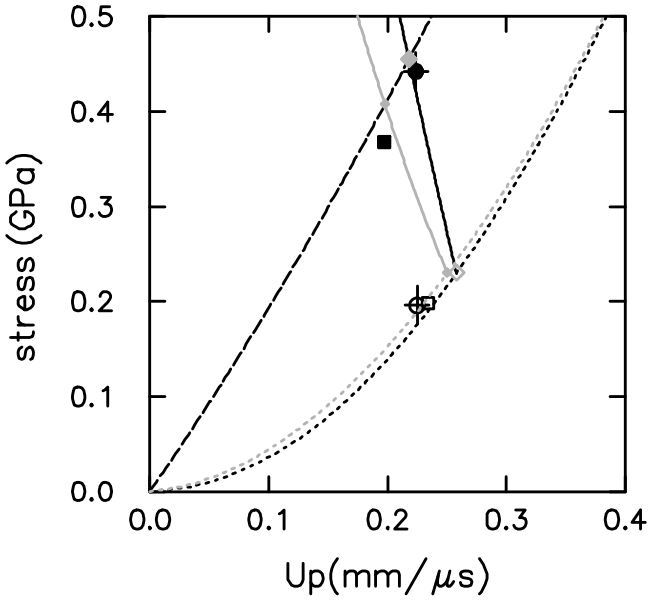

FIG. 11. Wave curves for impedance match at back interface of sample assuming burn increases pressure of incident shock from 0.19 GPa to 0.23 GPa. Lines and symbols have the same meaning as in previous figure.

assumption is valid for the simulation but not for the experiment. The front gauge data shows a slow rise in the stress and a decrease in the velocity.

The gauge record suggests that the compaction wave triggers a small amount of decomposition. The wave strength, as measured by the stress, increases by 15 %, from 2 kb to 2.3 kb. The impedance match with this strength for the incident compaction wave is shown in figure 11. We note that the assumptions — the wave strengthens as it propagates and there is no porosity behind the compaction wave — lead to good agreement with both the experimental wave speed of the incident compaction wave and the reflected wave strength at the back boundary.

The amount of burn needed to increase the compaction wave strength can be estimated from the assumption that the gaseous products and the solid HMX are in pressure equilibrium. Constant volume burn for HMX results in a pressure of about 150 kb. The high pressure gaseous products then expands until it reaches the compaction wave pressure, 2.3 kb. The expansion can be estimated from the adiabatic exponent, $2.3/150 = (\rho_g/\rho_s)^\gamma$. Assuming an average value of $\gamma \approx 2$, the gaseous products expand 8 fold. Let the mass fraction of burnt HMX be λ. Then the expanding gas compresses the solid by an amount $V/V_0 = (1 - \frac{\rho_s}{\rho_g}\lambda)/(1-\lambda)$. The pressure rise of 0.3 kb is given by $(1 - V/V_0)K = (\rho_s/\rho_g - 1)\lambda/(1-\lambda)K$. Using for the bulk modulus $K = 130$ kb, gives a value for the burn fraction of less than 1 %.

Treating the grains as inert is the likely explanation of the discrepancy between the simulated results and the experimental data. With the resolution used in the simulation, the needed burning would correspond to only 1 cell per grain. Such a small amount of burning would be difficult to compute accurately.

V. FINAL REMARKS

The meso-scale simulations of compaction waves agree fairly well with the gauge data from gas gun experiments. Moreover, other simulations with twice the resolution (5 micron cell size) give essentially the same results. Thus, the average mechanical behavior of a compaction wave in a granular bed can be simulated fairly well.

We conclude with a discussion of two issues. The first is the low yield strength needed to match the experimentally measured compaction wave speed. The second is the topic of including burn in the simulations. Reactive simulations are needed in order to understand the initiation process sufficiently well to develop better burn models. In particular, meso-scale simulations should be able to determine the extent to which dissipative energy can be localized, and thus the size and peak temperature of a hot spot.

A. Yield strength

The compaction dynamics is determined by the plasticity model describing the strength of the grains. The condition for plastic flow used here is based on a von Mises yield strength. The yield strength inferred from wave profile experiments in a single crystal of HMX [7,8] is 2.6 kb. This is compatible with the crush-up pressure in quasi-static compression experiments [9] and with experience from pressing HMX based plastic-bonded explosives, namely, after pressing to a pressure of 20,000 psi (1.4 kb) a porosity of a few per cent still remains. On the other hand, the yield strength of 1.3 kb inferred from hardness measurements [10,11] is half the value obtained from the wave profile experiments. This discrepancy may be related to the preferred slip directions within the crystal and the extent to which different stimuli couple to those slip directions. Simulations with the lower value of yield strength agree with the experiment analyzed here. But there are other factors to consider.

Stress bridging is observed to occur under a static elastic load. It also can be seen in the stress field behind the compaction wave, figure 4a. As the load is increased, stress concentrations at the contacts between grains gives rise to localized plastic flow. Several factors affect the stress concentrations. One is the distribution of grain sizes and the way in which grains are packed. Typically, the grains have a log-normal distribution. To achieve lower porosities in plastic bonded explosives, bimodal distributions are used. For our simulations, the grains have a variation in radius of 10 % with a uniform distribution. This choice is based on the computational cell size which did not allow small grains to be resolved adequately. In addition, the stress concentrations depend on the dimensionality. The calculations are two-dimensional while in reality the granular bed is three-dimensional. All of these factors affect the porosity behind a compaction wave.

Finally, we note additional gas gun experiments [1, Fig. 2.8] in which the projectile had the same impact velocity. With the same porosity but fine grains (average size of 10 to 15 micron), the transit time of the compaction wave across the granular bed is 0.8 μs less than with the coarse grains (average size of 120 micron). This raises the wave speed by 14 %. The wave speed is than comparable to the value predicted by the simulation with the yield strength based on the wave profile experiments. Two other experiments with a lower porosity (26 % rather than 35 %), one with fine grains and the second with coarse grains, have the same transit time. Based on the velocity at the back gauge, we can infer decomposition occurs only in the experiments with coarse grains. Gauge records for other experiments at a higher impact velocities show a substantial amount of decomposition [1, Fig. 2.14]. Again the amount of decomposition depends on the grain size.

B. Issues with burn

The mechanical properties of a compaction wave are largely determined by the jump conditions derived from the conservation laws. The heterogeneities, on average, only affect the width of the wave profile. In contrast, fluctuations caused by the heterogeneities are important for reactive materials. Because chemical reaction rates are strongly temperature dependent, the burn rate is determined by hot spots, *i.e.*, the tail of the temperature distribution. The size and peak temperature of hot spots are affected by details of the model and are more difficult to simulate accurately. The nature of the heterogeneities — grain size distribution, two-dimensional vs. three-dimensional packing and orientation of anisotropic crystalline grains — can be expected to affect the temperature distribution. In addition, the dissipative mechanisms that give rise to the wave profile are important.

The simulations reported here include three dissipative mechanisms: (i) plastic work, (ii) shear viscosity, and (iii) artificial viscosity. In addition, other simulations were performed with a rate dependent plasticity model. The dissipation occurs mainly near interfaces between grains. The peak temperatures depend on how small a volume the dissipative energy is localized in, and for a simulation is affected by the resolution. With the resolution of our simulations, the peak temperatures are below the melt temperature of HMX. Temperatures above melting are needed for significant decomposition to occur on the micro-second time scale of the gas gun experiments. Thus, burning wouldn't have occurred even if the simulations included a reaction rate.

One dissipative mechanism that is conspicuously absent from our simulations is frictional heating at grain boundaries. The dilemma is that in order to calculate large distortion of the grains, Eulerian algorithms smear out interfaces with mixed cells and thus make it difficult to account for physical effects at interfaces. In addition, the estimate of the resolution needed for frictional heating is sub-micron [12] and would be computationally impractical without a subgrid model. Similarly, deflagration wave fronts initiated by hot spots are very thin and would require a subgrid model.

For stronger waves (stress much larger than the yield strength) the dominant heating mechanism is undoubtably due to the implosion of the pores or void collapse. Depending on the Reynolds number, void collapse leads to either viscous heating or micro-jetting (which generates heat when the jet stagnates on the back surface of the pore). Both viscous heating and micro-jetting can produce hot spots with sufficiently high temperatures to achieve large reaction rates. The required resolution would depend on the pore size and is likely less stringent than is needed for dissipative mechanisms that dominate weak waves.

ACKNOWLEDGMENT

The author thanks Prof. David Benson for making his code available, and Drs. Richard Gustavsen and Stephen Sheffield for sharing the data from their experiments.

REFERENCES

[1] S. A. Sheffield, R. L. Gustavsen, and M. U. Anderson, in *High-pressure shock compression of solids IV: response of highly porous solids to shock compression*, edited by L. Davison, Y. Horie, and M. Shahinpoor (Springer-Verlag, NY, 1997), Chap. 2, pp. 23–61.

[2] D. J. Benson, in *High-pressure shock compression of solids IV: response of highly porous solids to shock compression*, edited by L. Davison, Y. Horie, and M. Shahinpoor (Springer-Verlag, NY, 1997), Chap. 9, pp. 233–255.

[3] D. J. Benson, V. F. Nesterenko, F. Jonsdottir, and M. A. Meyers, J. Mech. Phys. Solids **45**, 1955 (1997).

[4] J. M. McAfee, B. Asay, W. Campbell, and J. B. Ramsay, in *Ninth (International) Symposium on Detonation, Portland, OR, Aug. 28, 1989* (OCNR 113291-7, Office of the Chief of Naval Research, Arlington, VA, 1989), pp. 265–279.

[5] R. Menikoff and E. Kober, Technical Report No. LA-13546-MS, Los Alamos National Lab., (unpublished), available at http://lib-www.lanl.gov/la-pubs/00326750.pdf and http://lib-www.lanl.gov/la-pubs/00326751.pdf.

[6] R. Menikoff and E. Kober, in *Shock Compression in Condensed Matter–1999* (American Institute of Physics, NY, 1999), pp. 397–400.

[7] J. J. Dick, A. R. Martinez, and R. S. Hixson, Technical Report No. LA-13426-MS, Los Alamos National Lab., available at http://lib-www.lanl.gov/la-pubs/00418374.pdf.

[8] J. J. Dick and R. Menikoff, Technical Report No. LA-UR-01-574 (in preparation), Los Alamos National Lab.

[9] W. L. Elban and M. A. Chiarito, Powder Technology **46**, 181 (1986).

[10] V. K. Mohan, V. C. J. Bhasu, and J. E. Field, in *Ninth (International) Symposium on Detonation, Portland, OR, Aug. 28, 1989* (OCNR 113291-7, Office of the Chief of Naval Research, Arlington, VA, 1989), pp. 1276–1283.

[11] S. J. P. Palmer and J. E. Field, Proc. Roy. Soc. London **A 383**, 399 (1982).

[12] R. Menikoff and T. Sewell, Combustion Theory and Modelling, (submitted), available at http://t14web.lanl.gov/Staff/rsm/preprints.html#HMXMeso.